JOURNAL OF OPTOELECTRONICS AND ADVANCED MATERIALS, Vol. 12, No. 5, May 2010, p. 1035 - 1044

Optical characterization and thickness estimation of Al^{3+} ion doped ZnO nano-films from transmittance spectra

D. K. MADHUP[a,b*], D. P. SUBEDI[a], S. P. CHIMOURIY[a]
[a]*Thin Film and Plasma Science Laboratory, Kathmandu University, Dhulikhel, Kavre, Nepal.*
[b]*College of Biomedical Engineering and Applied Sciences, Hadigaun, Kathmandu, Nepal*

Al^{3+} ion doped and un-doped ZnO thin films deposited by nebulized spray pyrolysis method have been studied in the present work. The transmittance spectrum from UV-VIS-NIR spectrophotometer in 200 to 1100 nm wavelength range was used to retrieve the optical parameters: Optical band gap, Refractive index, Dielectric constant, Packing density, Dissipation factor, Optical conductivity, Relaxation time, carrier concentration to effective mass ratio, plasma frequency and Thickness for all films. Instead of entire Swanepoel algorithm, we used minimization approach which is appropriate to achieve an absolute optical properties and thickness as well, from the transmittance spectra even if it devoid of enough interference fringes. The analysis of the optical data revealed that the percentage of transmittance decreases gradually and there is widening of optical band gap to certain percentage of Al doping inside the ZnO. However, the other optical parameters showed dominant characteristics only at 3 mol% of Al^{3+} doping inside the ZnO.

(Received April 1, 2010; accepted May 26, 2010)

Keywords: ZnO, Spray Pyrolysis, UV-VIS-NIR spectrophotometer, Transmittance

1. Introduction

Zinc oxide thin films continue to attract wide spread scientific attention because of its low toxicity as opposed to indium coated tin oxide film. These can be used in fabricating a variety of devices including phosphor for color displays "Vanheusden *et al* [1]" and electrode material in LED and photovoltaic cells "Jiang et al [2]", gas sensors "Lin *et al* [3]" and varistors "Sato & Takada [4]." A transparent conductive oxide (TCO) layer is used as anode "Hartnagel *et al* [5]." Due to its high conductivity, suitable work function and transparency in the visible spectral range "Seki *et al* [6]" tin-doped indium oxides (ITO) are the most widely used TCO films. The problem is that Indium is a relatively scarce element in the earth's crust, which implies that ITO is a costly material. The other drawback of ITO films is being its chemical instability in a reduced ambient: the indium of ITO layer can simply diffuse into the organic materials, leading to degradation of LED performance. Besides, the toxic nature of indium could be hazardous to both human health and environment. These entail that LED industry is in a need for a better electrode material with improved device performance and lower production cost.

On the other hand, ZnO films are more stable in reducing ambient, more abundant and less expensive as opposed to ITO. In the past, Al and Ga ion doped transparent conductive zinc oxide films have been extensively examined as an alternative to ITO films "Coutts *et. al.* [7]." As a wide band gap photoelectric material, ZnO has unique electrical and optical properties, such as low dielectric constant, high chemical stability, and good photoelectric and piezoelectric behaviors. Zinc oxide, with a direct bandgap of 3.37 eV and an exciton binding energy of 60 meV, is a promising semiconductor for the fabrication of ultraviolet light-emitting diodes suitable for operation in harsh reduced environments and at high temperatures. ZnO has a number of advantages compared to those in other wide-band semiconductors such as GaN, SiC. These include higher quantum efficiency, greater resistance to high-energy radiation, and the possibility of wet chemical etching. However, despite much progress in ZnO technology in recent years, high-quality *p*-type ZnO and therefore, the manufacture of ZnO homojunctions, continues to be problematic. The properties of ZnO might be best exploited by constructing heterojunctions with ZnO active regions; in this way, the emission properties of an LED can still be determined by the advantageous properties of ZnO.

The problem is that ZnO itself suffers from the lack of a reproducible, high-quality, *p*-type epitaxial growth technology. Although much progress has been made in this area, the fabrication of effective ZnO-based devices is a challenging work, in terms of reproducibility. Currently, however, several groups have demonstrated good-quality *p*-type GaN (*p* GaN) and used these in fabricating LED thin film junction consisting of *n* ZnO with *p* GaN in combination "Chu *et. al.* [8]." The advantage of ZnO/GaN LEDs is that these heterostructure-based devices exhibit improved current confinement compared to homojunctions, which leads to higher recombination and improved device efficiency "Battaglia & George, Migliore [9-10]." The present work aims at casting aluminum doped zinc oxide films of improved quality. The advantage is that the optical and properties of TCO films can be controlled and tailored by optimizing fabrication conditions, matrix compositions and sintering temperature "Minami [11]."A variety of methods have been developed

for the preparation of ZnO thin films. These include thermal evaporation "Sato & Sati [12]", rf sputtering "Shih & Wu [13]", chemical vapor deposition "Natsume [14]", laser ablation "Dinesscu, P Verardi [15]", spray coating "Studemikin [16]" and dip-coating "Radhouane, & Maity *et. al.* [17-18]."

The interest arase in spray coating method in fabricating thin films springs from a number of practical considerations. Among other, these include its simplicity and room temperature based solution chemistry, which helps homogenous mixing of chemicals, yielding homogeneous distribution of dopant ion on host matrix. Secondly, since it does not require vacuum it is very economic as opposed to chemical vapor deposition technique and rf sputtering technique. Also, it can be adapted for making large-area films such as those employed in display technology.

Numerous investigations were reported on optical properties of Al ion doped and un-doped ZnO films prepared by several techniques. However, our study of already performed investigations found that there are several variation as well as missing on some major optical constraints of both Al doped and un-doped ZnO films. Furthermore, ZnO based thin films have not analyzed previously, their complete optical properties in UV region as it has several medical applications [19, 20]. Hence in this work, we tried to cover and elaborate those missed optical constraints by simple way. Previously reported results by "Pal *et.al.* [21]" have been found to have flaw in mathematical expression derived from KK model. Consequently, all the results obtained from that expression have to have imperfection. So here in this communication, we tried to elaborate the modified form of the mathematical expression with brief description and presented the results for Al doped ZnO films obtained by using newly derived expression.

2. Mathematical and computational methods

The real part of the refractive index as a function of wavelength, n (λ) of a semiconductor material can be related to the optical absorption coefficient α (λ) as described by "Kramer's Kronig (KK) model [22]" shown in Eq. (1).[Pankove, 1971, P. 92]:

$$n(\lambda) = 1 + \frac{1}{2\pi^2}\int_0^{\infty} \frac{\alpha(\psi)}{1-\frac{\psi^2}{\lambda^2}} \qquad (1)$$

where φ is the running variable in the wavelength range $[0, \infty]$.

The KK model demand very wide range of wavelength of spectrophotometer to estimate the absorption coefficient for the determination of optical constants and accurate thickness of the film. However, any UV-VIS-NIR spectrophotometers only have the finite range of wavelength to estimate absorption coefficient. The spectral distribution of the absorption coefficient α of the film has been determined from the relation as expressed by Eq. (2) "Tan *et. al.* [23]":

$$\alpha = -\frac{\ln(T)}{d} \qquad (2)$$

where, T is the transmittance and d is the film thickness which is necessary to get exact optical properties of the film.

So, the wavelength range from $0 \text{ to } \infty$ used in KK relation is resolved in to three parts: one is in the range below the lower limit of UV-VIS-Spectrophotometer i.e $0 \text{ to } \lambda_1$ and another higher range which is above the highest limit of UV-VIS-Spectrophotometer i.e $\lambda_2 \text{ to } \infty$. And the range in between is the estimable wavelength range from $\lambda_1 \text{ to } \lambda_2$ which could be asserted by the UV-VIS-NIR Spectrophotometer. That is,

$$n(\lambda) = I_1 + I_2 + I_3$$

For I_1, We have

$$I_1 = \frac{A}{2\pi^2}\int_0^{\lambda_1} \frac{\left(\frac{hc}{\psi} - E_g\right)^{\frac{1}{2}}}{1-\frac{\psi^2}{\lambda^2}} d\psi \ ;$$

$$\text{Let } \frac{hc}{\psi} - E_g = x^2, \text{ i.e. } \psi = \frac{hc}{x^2 + E_g}, \text{ and}$$

$$d\psi = -\frac{hc}{\left(x^2 + E_g\right)^2} 2x\, dx$$

As $\psi \to 0, x \to \infty$ and as

$$\psi \to \lambda_1, x \to \sqrt{\left(\frac{hc}{\lambda_1} - E_g\right)} = x_1 \left(\text{say}\right); \text{ A is constant.}$$

If λ is greater than wavelength corresponds to band gap, then, $E_g > \frac{hc}{\lambda}$.

$$I_1 = \frac{A\lambda}{2\pi^2}\left[\left(P - Q\right)\frac{\pi}{2} - P\tan^{-1}\left(\frac{x_1}{P}\right) + Q\tan^{-1}\left(\frac{x_1}{Q}\right)\right] \qquad (3)$$

Where, $P^2 = E_g + \frac{hc}{\lambda}$ and $Q^2 = E_g - \frac{hc}{\lambda}$

If λ is less than wavelength corresponds to band gap, then, $E_g < \frac{hc}{\lambda}$.

$$I_1 = \frac{A\lambda}{2\pi^2}\left[C\frac{\pi}{2} - C\tan^{-1}\left(\frac{x_1}{C}\right) - \frac{D}{2}\ln\left(\frac{x_1 - D}{x_1 + D}\right)\right] \qquad (4)$$

Where, $C^2 = \frac{hc}{\lambda} + E_g$ and $D^2 = \frac{hc}{\lambda} - E_g$

For I_2, the estimable wavelength range from λ_1 to λ_2, the absorption coefficient can be calculated using Eq. 1 for any arbitrary value of d. Therefore,

$$I_2 = \frac{1}{2\pi^2} \sum_{\substack{\psi=\lambda_1 \\ \psi\neq\lambda}}^{\lambda_2} \frac{\alpha(\psi)}{\left(1-\frac{\psi^2}{\lambda^2}\right)} \Delta\psi \quad (5)$$

where $\Delta\psi$ is the computational steps

At the point $\psi=\lambda$, $\lim_{\psi\to\lambda} \frac{1}{2\pi^2} \frac{\alpha(\psi)\Delta\psi}{\left(1-\frac{\psi^2}{\lambda^2}\right)} = \frac{\alpha(\lambda)\lambda}{4\pi^2}$

For I_3, We have

$$I_3 = \frac{\alpha(\lambda_2)}{2\pi^2} \int_{\lambda_2}^{\infty} \frac{1}{1-\frac{\psi^2}{\lambda^2}} d\psi$$

Since λ is less than all ψ,

$$I_3 = -\frac{\alpha(\lambda_2)\lambda}{4\pi^2} \ln\left(\frac{\lambda_2+\lambda}{\lambda_2-\lambda}\right) \quad (6)$$

Finally, adding the values of I_1, I_2 and I_3 as depicted in Eq. (3), (4), (5) and (6), the real part of the refractive index may be asserted.

The wavelength dependent extinction coefficient K (λ) is found by the relation described by Eq. (7).

$$k(\lambda) = \frac{\alpha(\lambda) \times \lambda}{4\pi} \quad (7)$$

The findings of real and imaginary parts of refractive index invoke us to estimate the transmittance for arbitrary value of film thickness by applying the Swanepoel equation, referred to as T_{calc}. Then, after the minimization between measured and calculated transmittance for arbitrary value of film thickness by iterative method, exact film thickness can be calculated. Knowing the exact value of the film thickness, the real and imaginary part of the refractive index could be determined which bring in to play to estimate the other interrelated optical constants as described in this communication for Al doped ZnO films.

3. Experimental detail

The syntheses of ZnO and Al^{3+} ion doped ZnO (AZO) films have been performed by using ultrasonic spray nebulizer [SONAER]. This apparatus is capable of spraying a gel like solution at continuous and constant flow rate so as to get a film of very smooth surface. The starting material used in our experiment was dehydrated zinc acetate and the substrate material was quartz.

We prepared a 0.1M aqueous solution of zinc acetate in ethanol as the precursor of the thin film. To dope aluminum, we used aluminum acetate solution prepared in ethanol and mixed with 0.1M zinc acetate solution at different molar concentration varying from 1 to 10 mol %. Few drops of acetic acid was added in the final solution to get complete dissociation of zinc acetate and then stirred with magnetic stirrer at 60^0C for 10 minutes to obtain clear homogeneous solution. The homogeneous solution was kept in ultrasonic vibrator for 10 minutes just before the deposition.

The Al doped and un-doped zinc acetate solution was deposited on quartz substrate cleaned ultrasonically with ethanol and initially heated to a temperature of 500 ± 10^0 C. But, during the deposition the substrate temperature falls to 325 ± 10^0 C. The measurement of substrate temperature was obtained by K-type thermocouple probe as well as laser temperature detector and maintained constant with temperature controlled electric heater. The thicknesses of all films were maintained constant in certain range by controlling flow rate and sprayed volume. The flow rate of the solution throughout the experiment was maintained at 5 ml per minute, keeping the spray nozzle 20 cm away from the substrate. The prepared films were dried at 500^0C for 2 minutes just after the deposition so as to evaporate the solvent and to increase the smoothness of the film surface.

4. Results and discussion

4.1. Transmittance as a function of wavelength

Spectral distribution of transmittance as a function of wavelength T(λ) from UV region-200 nm to NIR-1100 nm was studied using spectrophotometer (GENESYS UV-10). The spectra were retrieved at 1 nm wavelength interval at room temperature. The observed transmittances are about 90 to 97% in the visible region for un-doped and Al doped thin film as shown in Fig. 1, which is important for its application such as transparent conducting films and solar cell windows "Yang *et. al*. and sang *et. al.* [24, 25]."

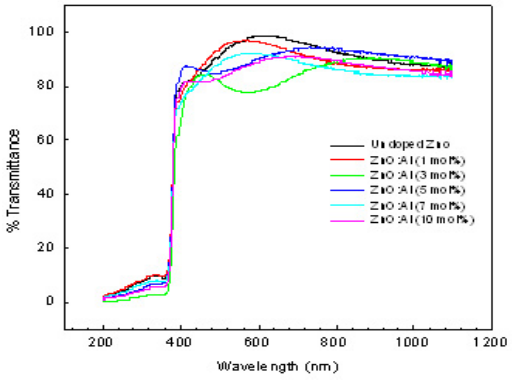

Fig. 1. Spectral distribution of transmittance as a function of wavelength for different doping (Al) concentration varying from 1-10 mol %.

Moreover, in the UV region the transmittance is near to zero and increases with the wavelength towards the visible region for all doped and un-doped films. The high value of transmittance is probably due to the existence of an interfacial layer with very low refractive index between the film and substrate "Porqueras *et. al*. [26]"

The interference fringes in the spectra reveals that all the doped and un-doped ZnO film are optically smooth surfaces and that the interface with the quartz substrate is also smooth.

4.2. Film thickness

The thickness can be obtained from transmittance spectra quite accurately with the so called envelop method "Manifacier *et. al*., Goodman *et. al*., Swanepoel *et. al*. [27-30]." The main shortcoming of such methods, however, is that they can't be used in the case of rather thin films, because their transmittance doesn't contain an enough interference fringe pattern to apply the envelop method. So, to estimate the thickness of the film, we applied a minimization approach (described in section 2.) between the measured transmittance by spectrophotometer and calculated transmittance from Swanepoel equation [29, 30] for different arbitrary values of thickness. The obtained values of thickness for doped and un-doped ZnO for different doping concentration are shown in Fig.2.

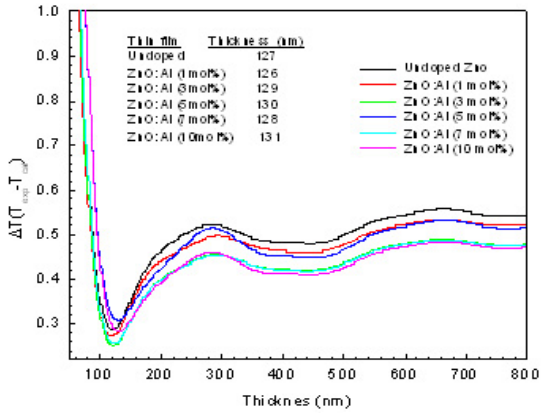

Fig. 2. ΔT (T_{exp}-T_{cal}) vs. thickness (nm) for different doping concentration varying from 1-10 mol %.

4.3. Absorption coefficient and optical band gap

The obtained values of absorption coefficient already expressed in Eq. 1 were used to determine the optical band gap. By applying the Tauc model "Tauc *et. al*. [31]" and the Davis and Mott model "David and Mott *et. al*. [32]" in the high absorption region described by Eq. (8):

$$\alpha h\upsilon = D\,(h\upsilon - E_g)^n \qquad (8)$$

where hυ is the photon energy, E_g is the optical band gap and D is a constant which doesn't depend on the photon energy and has a four numeric values, n = 1/2 for allowed direct, 2 for allowed indirect, 3 for forbidden direct and 3/2 for forbidden indirect optical transition. As ZnO is a direct band gap semiconductor material, n = 1/2 is found to be more suitable for ZnO thin film since it gives the best linear curve in the band-edge region "Tan *et. al*., Lu *et. al*. [23, 33]."

Applying the least square method to ensure linearity behavior of the curve $(\alpha h\upsilon)^2$ vs. hυ, the value of E_g was obtained by extrapolating the linear portion to the photon energy axis as explained elsewhere [23].

We found that the optical gap increases with the percentage of doping concentration up to 5 mol% and random variation on further increase of Al doping as shown in Fig. 3. As some researchers mentioned that only widening in band gap of ZnO with Al doping, this results shows controversial with the previously reported results of Al doped ZnO films. This may be due to the deformation of crystallanity of ZnO which invoke further investigations. For undoped ZnO the bandgap is 3.2508 eV whereas it increased to 3.2608 eV for 1 mol% of doping, 3.2663 eV for 3 mol% of doping, 3.2747 eV for 5 mol% of doping whereas the band gap is 3.2601 eV for 7 mol% of doping and 3.2724 eV for 10 mol% of doping.

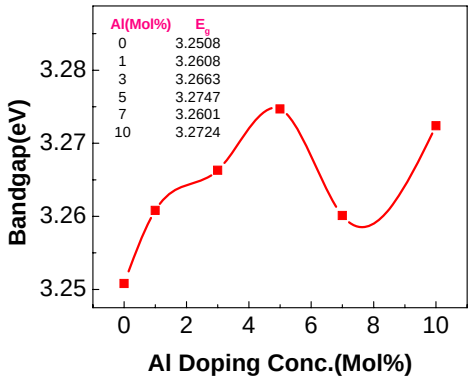

Fig. 3. Band gap of ZnO film as a function of Al doping concentration.

The obtained optical band gap from Fig. 4 concentrates on the electron density and the so called band effective mass described by Eq. (9).

$$E_g = E_{g\,o} + \frac{h^2 n^{2/3}}{8\pi^{2/3} m^*_{eff}} \qquad (9)$$

where $E_{g\,o}$ is the fundamental direct band gap, n and m^*_{eff} are the density and the effective mass of electron respectively. The second term is called Burstein-Moss; the latter contributes in the gap enlargement ΔE known as Moss-Burstein energy. This expression suggests that the optical gap is broadened as the free charge carrier concentration enhances as reported by "Benouis *et. al*. [34]" for their indium doped ZnO films.

The doping effect is associated with the excess of Zinc atom acting as a donor. The point defects can be

interstitials or oxygen vacancies. The free electron increases in proportion with the doping atoms increasing in the film network. The impurities are singly ionized and the associated electrons occupy the bottom of the conduction band as a free electron gas "Jin *et.al*. [35]."

4.4. Complex refractive index

As discussed before, the value of thickness was asserted using minimization approach. The absorption coefficient was also determined. Once the value of thickness and absorption coefficient are determined, the obtained values of real and imaginary part of refractive index have been plotted as shown in Fig. 4 and 5 respectively.

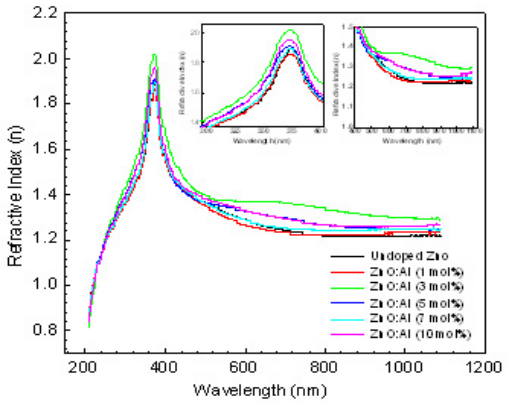

Fig. 4. Refractive index vs wavelength for different doping concentration varying from 1-10 mol %.

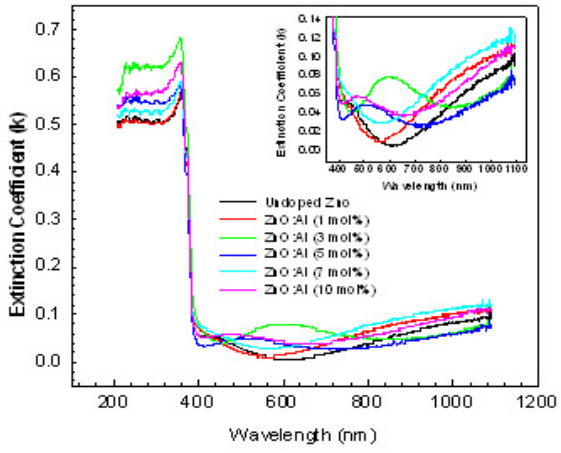

Fig. 5. Extinction coefficient vs wavelength for different doping concentration varying from 1-10 mol %.

The lower value of refractive index in the visible region reflects the low absorption in this region which shows good agreement with transmittance spectra. The existence of this low refractive index interfacial layer can be attributed to the singular ear structure, which could grow from the first nucleation.

Moreover, many researchers reported that the change in refractive index of ZnO film with the wavelength occurs only in the visible region but not in the UV region. Here, in this communication, we have mentioned the nature of the change in refractive index in the UV region which shows very peculiar characteristics in this region and our achievements is tailed quite well with the results reported by "Debnath *et. al*. [36]" for their CeO_2 thin films. The variations in refractive index depend not only on the wavelength but also on the doping concentration as shown in Fig. 14.

Furthermore, the refractive index of the film increases with increasing doping concentration up to 3 mol% and decreases thereafter as shown in Fig. 14. This increase in refractive index can be attributed to the increase in packing density with the concentration. The packing density of the film can be estimated from the Eq. (10). **"**Macleod *et. al*. [37]":

$$n_f^2 = \frac{(1-P)n_V^4 + (1+P)n_V n_S^2}{(1+P)n_V^2 + (1-P)n_S^2} \tag{10}$$

where, n_f is the refractive index of AZO film, n_s is the refractive index of the solid part of the film, that for single crystal, n_v is refractive index of voids (equals one for air), and P is the packing density. Therefore, the packing density P can be explained by Eq. (11).

$$P = \frac{(n_s^2+1)(n_f^2-1)}{(n_s^2-1)(n_f^2+1)} \tag{11}$$

The spectral distribution of packing density is shown in Fig. 6 whereas Inset of Fig. 6[a] shows their change with doping concentration.

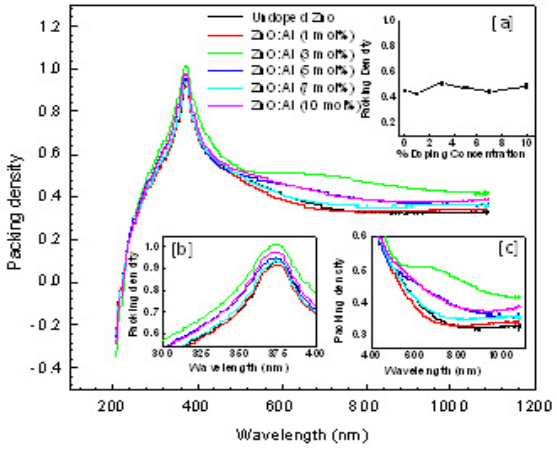

Fig. 6 Packing density vs wavelength for different doping concentration varying from 1-10 mol %.

It has been found that the estimated value of packing density increases with increasing Al doping concentration up to 3 mol%. This could be correlated to the decrease in

transmittance with increasing doping level. The decrease in refractive index after 3 mol% may be due to the excess increase in dopant ion which deteriorates the crystallinity of films, which may be due to the formation of stresses by the difference in ion size between zinc and the dopant and the segregation of dopant in grain boundaries for high doping concentration.

4.5. Complex dielectric constant

Optical properties of TCO'S in the longer wavelength region , where plasma edge occurs, is based on Maxwell's equations and Drude theory of free electrons. A complex permittivity that is function of frequency and conductivity can be defined using Maxwell's equations. From the complex permittivity and conductivity, expressions are derived for the real and imaginary part of the permittivity as a function of the material parameters. The plasma resonance frequency ω_p can be determined from the spectral dependence of these expressions of the dielectric constant, which are given by Eq. (12) and Eq. (13).

$$\varepsilon_1 = n^2 - k^2 = \varepsilon_\infty - \left(\frac{e^2 N}{4\pi^2 C^2 \varepsilon_0 m^*} \right) \lambda^2 \qquad (12)$$

$$\varepsilon_2 = 2nk = \left(\frac{\varepsilon_\infty \omega_p^2}{8\pi^2 c^3 \tau} \right) \lambda^3 \qquad (13)$$

where, ε_1 is the real part, ε_2 is the imaginary part of the dielectric constant, ε_∞ is the high frequency dielectric constant, ω_p is the plasma frequency, τ the optical relaxation time and $k = \frac{\alpha \lambda}{4\pi}$. The real and imaginary parts of the dielectric constant can be calculated as it is directly related to the density of states within the forbidden gap of the investigated sample "El-Korashy *et. al*. and Wakad *et. al*. [38,39]." The real and imaginary part of the dielectric constant of the films is shown in Fig. 7 and Fig. 8 respectively and their insets shows the enlarge version of the same figures.

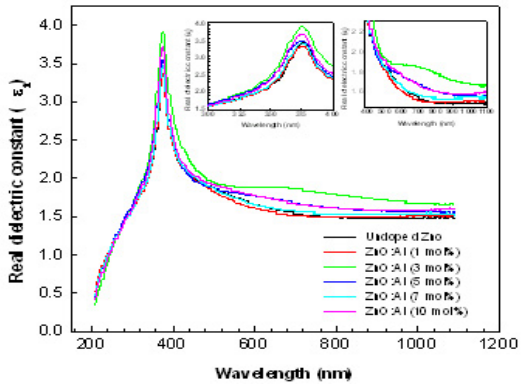

Fig. 7. Real part of dielectric constant vs. wavelength for different doping concentration varying from 1-10 mol %.

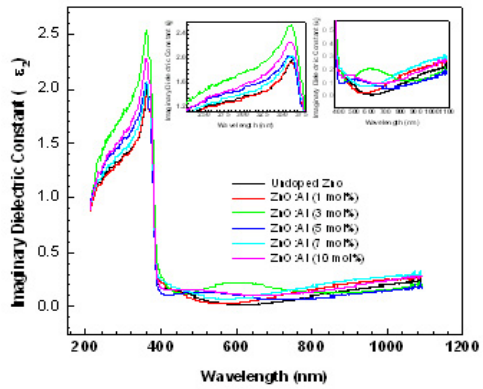

Fig. 8. Imaginary part of dielectric constant vs. wavelength for different doping concentration varying from 1-10 mol %.

It has been found that the imaginary part of dielectric constant decreases sharply in the visible region and the value is near to zero. The low value of ε_2 indicates low dielectric loss in the obtained films.

4.6. High frequency dielectric constant

The determined refractive index for doped and un-doped ZnO film is analyzed to obtain their high frequency dielectric constant via procedures "Zemel *et. al*. [40]" describes the contribution of the free carriers and the lattice vibration modes of the dispersion. The high frequency dielectric constant has been reported by "Zemel *et. al* [40]"as described by Eq. (14).

$$\varepsilon_1 = \varepsilon_\infty - B\lambda^2 ; \; B = \frac{e^2 N}{4\pi^2 C^2 \varepsilon_0 m^*} \qquad (14)$$

where, ε_1 is the real part of dielectric constant, ε_∞ is the high frequency dielectric constant, N the free charge carrier concentration, ε_0 the permittivity of the free space (8.85×10^{-12} F/m), m^* the effective mass of the charge carrier and C the velocity of light.

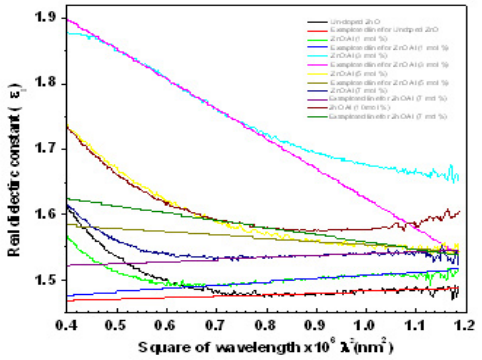

Fig. 9. Real part of dielectric constant vs. square of wavelength for different doping concentration varying from 1-10 mol %.

Earlier obtained value of ε_1 as a function of wavelength λ is re-plotted as a function of λ^2 as shown in Fig. 9.

It has been found that the trace of ε_1 versus λ^2 is linear at longer wavelengths. Applying the least square method to ensure linearity behavior of the determined curve, extrapolate the best fit curve to zero wavelength gives the value of ε_∞ and from slope of these lines, Value of $\frac{N}{m^*}$ for the measured sample was determined according to Eq.10 of constant B.

In a semiconductor the carrier concentration (N) varies according to the plasma frequency ω_p as "Pankove, PP 89, Manifacier *et. al*. 1977, Lyden *et. al*., Ferry. Ch 5, [41, 42-44]" described by Eq. (15).

$$\omega_p = \sqrt{\frac{N e^2}{m^* \varepsilon_0 \varepsilon_\infty}} \tag{15}$$

4.7. Dissipation Factor

Loss-rate of power of a mechanical mode, such as an oscillation in dissipative system can be measured by dissipation factor. For example, electric power is lost in all dielectric materials, in the form of heat, light, sound etc. The dissipation factor $\tan\delta$ can be calculated according to the Eq. (16). "Yakuphanoglu *et. al*. [48]":

$$\tan\delta = \frac{\varepsilon_2}{\varepsilon_1} \tag{16}$$

The variation of dissipation factor of the fabricated films as a function of wavelength is shown in Fig.10. It is found that the dissipation factor value is high in the UV region and decreases sharply at 400 nm and saturating after that up to 1100 nm. However, the wavelength near to the band gap energy, the value of $\tan\delta$ decreases sharply near to zero. Finally it's constant in whole visible region.

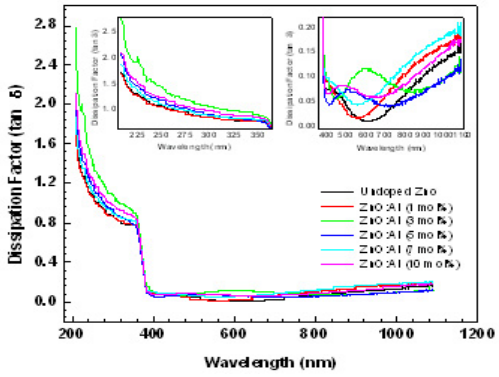

Fig. 10. Dissipation factor vs wavelength for different doping concentration varying from 1-10 mol %.

4.8. Optical Conductivity

The optical conductivity σ_{opt} can be defined in terms of absorption coefficient α as follow with Eq. (17). "Pankove, P. 91, [49]":

$$\sigma_{opt} = \frac{\alpha\, n\, c}{4\,\pi} \tag{17}$$

Fig. 11 shows the variation of optical conductivity σ_{opt} as a function of photon energy. We found that the optical conductivity is low for low value of photon energy and increases drastically from the energy corresponding to band gap energy.

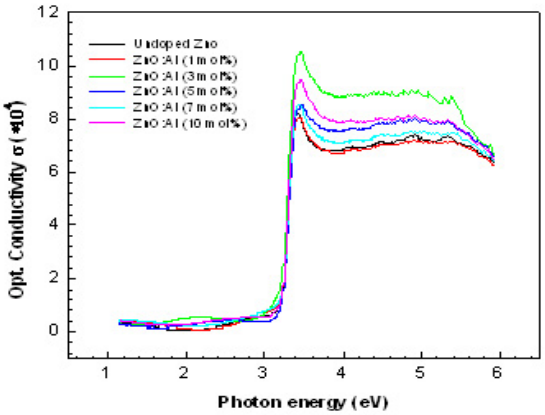

Fig. 11. Optical conductivity vs. wavelength for different doping concentration varying from 1-10 mol %.

Increase in optical conductivity at high photon energies is due to high absorbance of doped and un-doped ZnO film. It may be due to the electron excited by photon energy "Yakuphanoglu *et. al*. [50]."

Optical conductivity as a function of Al doping concentration is shown in Fig. 13(d), which shows good agreement with $\frac{N}{m^*}$ versus Al doping concentration plot [Fig.13(b)].

4.9. Relaxation time

The properties of a dielectric change on a time scale is determined by the relaxation time when an external electric field is changed. The dielectric relaxation time is a property of a solid that is closely related to its conductivity.

The dielectric relaxation time is a measure of the time it takes for charge in a semiconductor to become neutralized by conduction process. The dielectric relaxation time τ can be evaluated by using the relation shown in Eq. (18). "Abdel-Aziz *et. al*., Bell *et. al*., Han *et. al*. [51-53].

$$\tau = \frac{\varepsilon_\infty - \varepsilon_1}{\omega\, \varepsilon_2} \qquad (18)$$

Fig. 12 shows the dielectric relaxation time as a function of wavelength λ for doped and un-doped ZnO film.

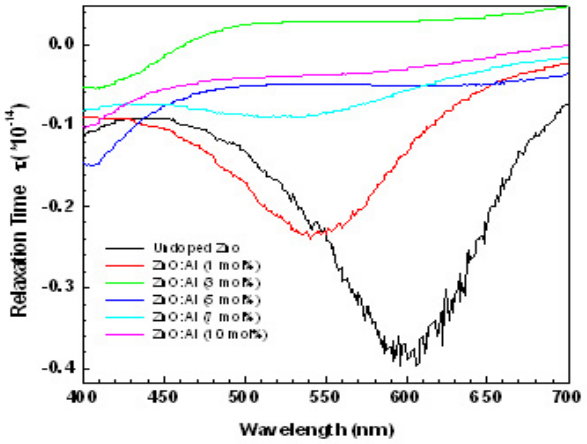

Fig. 12. Relaxation time vs wavelength for different doping concentration varying from 1-10 mol %.

It is found that the relaxation time increases with the incorporation of Al inside the ZnO and has a maximum value at 3 mol%, it may be due to the excess carrier concentration on this concentration. This maximum can also be tailed with the parameters like ε_∞, $\frac{N}{m^*}$ and ω_p which has a similar effects.

4.10. Effect of doping concentration

The obtained value of high frequency dielectric constant (ε_∞), ratio of charge carrier to their effective mass ($\frac{N}{m^*}$), plasma frequency (ω_p) and optical conductivity (σ_{opt}) are plotted as a function of doping concentration as shown in Fig.13 [a], [b], [c] and [d] respectively.

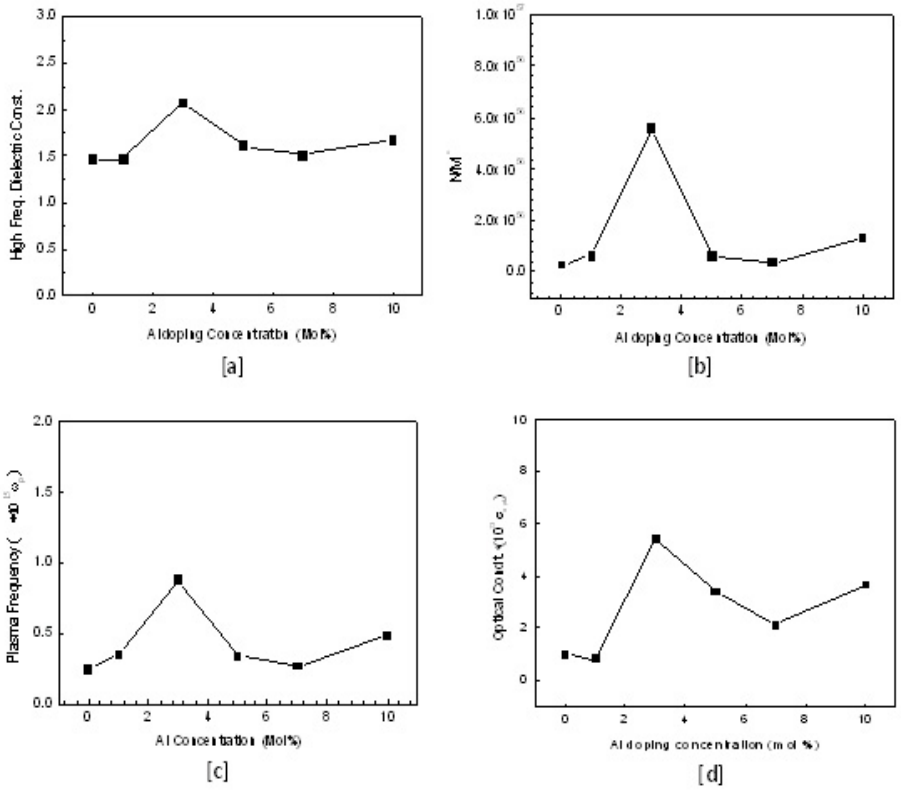

Fig. 13. Variation of [a] ε_∞ [b] $\frac{N}{m^*}$ [c] ω_p [d] σ_{opt} as a function of doping concentration.

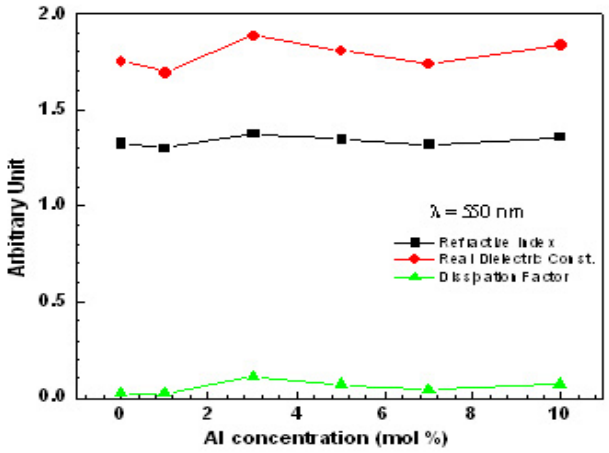

Fig. 14. Comparision of n, ε_1, and tanδ *as a function of doping concentration.*

Moreover, the parameters like refractive index, dielectric constant and dissipation factor depends not only on the wavelength but also on the doping concentration. Therefore, their relative comparison of the effect of addition of Al^{3+} ion inside the ZnO is depicted in Fig. 14.

It is found that all these parameters shows higher value at doping concentration of 3 mol%. This result shows good agreement with peak optical conductivity versus doping concentration.

The obtained results reveals that very high dose of doping concentration might not occupy the correct places inside the zinc oxide crystallites because of the limited solubility of aluminum inside ZnO. This result tailed quite well with the result obtained by "Alam *et.al*. [45]" for the determination of electrical conductivity, also tailed with the result reported by "Kuo *et. al.* [46]" for the findings of diffraction peak intensities.

Therefore, excess aluminum may occupy interstitial positions "Alam *et. al*., Cossement & Streydio *et. al*. [45,47]" leading to distortion of the crystal structure. Hence the dopant atoms become ineffective as donors, as the higher level of Al incorporation lead to interstitial incorporation of Al in the form of Al_2O_3 "Cossement & Streydio *et. al*. [47]" giving rise to the greater electron scattering. The aluminum atoms may also segregate to the grain boundaries in the form of Al_2O_3, which will increase the grain boundary barrier and hence the optical conductivity increases after a certain level of doping concentration.

4. Conclusions

Un-doped and doped with aluminum ZnO films of different doping concentration characterized by UV-VIS-NIR reached on the following conclusive remarks:

(i) Regarding the Al doping inside the ZnO in normal condition, the optical studies conclude that only certain percentage of Al can be doped to avoid the degradation of crystallinity of films.

(ii) The spectral distribution of refractive index reveals that it has sharp change in UV region for both un-doped and Al-doped films. However, 3 mol% doped films shows highest value of refractive index at mid-band of visible region and corresponding packing density were studied.

(iii) The investigation of dielectric constant for ZnO and ZnO:Al films performs that they gives low dielectric loss in visible region. However, the dissipation factor decreases sharply at 400 nm and constant after this.

(iv) The optical conductivity increases with photon energy. However, the effect of doping shows that 3 mol% doping concentration shows highest conductivity. This result tailed quite well with the obtained data of plasma frequency, N/m^* ratio and high frequency dielectric constant. Moreover, this dominant concentration has been proved by the results on relaxation time.

Acknowledgement

The authors would like to thank "Third World Academic of Sciences (TWAS)", ICTP,Italy, for financial support through a research grant No. 06-016 RG/PHYS/AS.

References

[1] K. Vanheusden, W L Warren, C H Seager, D R Tallant, J A Voigt, B E Gnade, J Appl Phys **79**, 7983 (1996).
[2] X. Jiang, F L Wong, M K Fung, T Lee, Applied Phys Latters **83**, 9 (2003).
[3] F. C. Lin, Y Takao, Y Shimizu, M Egashira, J Am Ceram Soc **78**, 2301 (1995).
[4] K. Sato, Y Takada, J Appl Phys **53**, 8819 (1982).
[5] H. L. Hartnagel, A. L. Dawar, A. K. Jain, C. Jagadsik, Semiconducting Transparent Thin Films, Institute of Physics, Philadelphia, (1995).
[6] S. Seki, Y. Sawada, T. Nishide, Thin Solid Films. **388**, 22 (2001).
[7] T. J. Coutts, D. L. Young, X. Li, Mater. Res. Bull. **25**, 58 (2000).
[8] Chen-Fu Chu, Fang-I Lai, Jung-Tang Chu, Chang-Chin Yu, Chia-Feng Lin, Hao-Chung Kuo, S. C. Wanga, J. App. Phys. **95**, 8 (2004).
[9] F. Battaglia and T. F. George, Fundamentals in Chemical Physic, Kluwer, Boston, (1998).
[10] L. Migliore, Laser Materials Processing, Markcel Dekker, New York, (1996).
[11] T. Minami, J. Vac. Sci. Technol. A **17**, 1765 (1999).
[12] Y. Sato, S Sati, Thin Solid Films. **281**, 445 (1996).
[13] W. C. Shih, M S Wu, J Crystal Growth. **137**, 319 (1994).
[14] Y. Natsume, H Sakata, T Kirayama, H Yanagida, J. Appl. Phys. **72**, 4203 (1992).
[15] M. Dinesscu, P Verardi, Appl Surf Sci. **106**, 149 (1996).

[16] S. A. Studemikin, N Golego, M Cocivera, J Appl Phys **83**, 4 (1998).
[17] Radhouane Bel Hadj Tahar, Journal of the European Ceramic Society. **25**, 14 (2005),
[18] R. Maity, S. Kundoo, K.K. Chattopadhyay, Solar Energy Materials and Solar Cells **86**, 2, (2005).
[19] M. Adeney, J. Oppenheim, A comparison of two physical light blocking agents for sunscreen lotions, Varian, UV-56, March 1992.
[20] Umicore, Nano-Sized Oxide Powder for UV Applications,Innovation for Sustainable Production (I-SUP 2008), Bruges 22-25 April 2008.
[21] S. R. Bhattachraya, R.N. Gayen, R. Paul, A.K. Pal, Thin Solid Films, **517,** 5530 (2009) .
[22] Pankove, Optical process in semiconductors, Prentice-Hall, Englewood Cliffs, NJ. 1971, P. 92.
[23] S. T. Tan, B.J. Chen, X. W. Sun, W. J. Fan, J. App. Phys. **98**, 013505 (2005).
[24] T. L. Yang, D. H. Jhang, J. Ma, H.L. Ma, Y. Chen, Thin Solid Films **326,** 60 (1998).
[25] B. Sang, A. Yamada, M. Konagai, Appl. Phys. (Jpn. J.) 37 (Part 2), L206 (1998).
[26] I. Porqueras, C. Person, C. Corbella E. Bertran Solid State Ionics **165**, 131. (2003).
[27] J. C. Manifacier, J. Gassiot, J. P. Fillard, J. Phys. E: Sci. Instrum. **9**, 1002 (1976).
[28] A. M. Goodman, Applied Optics **17**, 2779 (1978).
[29] R. Swanepoel, J. Phys. E: Sci. Instrum. **16**, 1214 (1983).
[30] R. Swanepoel, J. Phys. E: Sci. Instrum. **17**, 896 (1984).
[31] J. Tauc, Amorphous and Liquid semiconductors (Plenum, London, 1974).
[32] E. A. David, N. F. Mott, Philos. Mag. **22**, 903 (1970)
[33] J. G. Lu, Z. Z. Ye, L. Wang, J. Y. Hung, B. H. Zhao, Mater. Sci. Semicond. Proces. **5**, 491 (2003).
[34] C. E. Benouis, A. Sanchez-Juarez and M. S. Aida, J. App. Sci. **7**(2), 220 (2007).
[35] Jin, Z. C. et.al,. J. Applied Phys. **64,** 5117 (1988).
[36] S. Debnath, M. R. Islam, M. S. R. Khan, Bull. Mater. Sci. **30**(4), 315 (2007).
[37] H. A. Macleod, J. Vac. Sci. Technol. A **4**, 418 (1986).
[38] A. El-Korashy, H. El-Zahed, M. Radwan, Physica B **334**, 75 (2003).
[39] M. M. Wakad, E. Kh. Shokr, S. H. Mohammed, J. Non-Cryst. Solids **265**, 157 (2000).
[40] J. N. Zemel, J. D. Jensen, R.B. Schoolar, Phys. Rev. A. **140**, 330 (1965)
[41] Pankove, Optical process in semiconductors, Prentice-Hall, Inc, NJ, USA, PP. 89.
[42] J. C. Manifacier. M. De. Murcia, J. P. Fillard, E. Vicario, Thin Solid Films, **41,** 127 (1977).
[43] H. A. Lyden, Phys. Rev. **134**, A1106 (1964).
[44] D. K. Ferry, Semiconductors, Mc Millian, New York, 1995 Ch. 5.
[45] M. J. Alam, D. C. Cameron, ICECE 2002, 26 – 28, Bangladesh.
[46] Shou – Yi Kuo, Wei – Chun Chen, Fang – I Lai, Chin – Pao Cheng, Hao – Chung Kuo, Shng – Chung Wang, Wen – Feng Hsieh, J. Cryst. Growth, **287**, 78 (2006).
[47] D. Cossement, J. M. Streydio, J. Cryst. Growth, **72**, 57 (1985).
[48] F. Yakuphanoglu, A. Cukurovali, I. Yilmaz, Physica B **351**, 53 (2004).
[49] J. I. Pankove, Optical process in semiconductors, Dover Pub, Inc. New York, 1975, P. 91.
[50] F. Yakuphanoglu, A. Cukurovali, I. Yilmaz, Optical Materials **27**, 1366 (2005).
[51] M. M. Abdel-Aziz, I. S. Yahia, L. A. Wahab, M. Fadel, M. Afifi, Applied Surface Science **252**, 8163 (2006).
[52] R. J. Bell, M. A. Ordal, R. W. Alexender, Appl. Opt. **24**, 3680 (1985).
[53] M. Y. Han, H. Huang, C. H. Chew, L. M. Gan, X. J. Zhang, W. Ji, J. Phys. Chem. B **102**, 1884 (1998).

*Corresponding author: dineshmadhup@yahoo.co.in, deepaksubedi2001@yahoo.com